Preferred citation: H. Karema, J. Salmela, M. Tukiainen and H. Lepomäki. Prediction of Paper Formation by Fluidisation and Reflocculation Experiments. In **The science of papermaking**, *Trans. of the XIIth Fund. Res. Symp. Oxford, 2001*, (C.F. Baker, ed.), pp 559–589, FRC, Manchester, 2018. DOI: 10.15376/frc.2001.1.559.

PREDICTION OF PAPER FORMATION BY FLUIDISATION AND REFLOCCULATION EXPERIMENTS

Hannu Karema,[1] *Juha Salmela,*[1] *Maarit Tukiainen*[2] *and Hannu Lepomäki*[2]

[1]VTT Energy, Technical Research Centre of Finland
P.O. Box 1603, FIN-40101 Jyväskylä, Finland
[2]Metso Paper Oy, P.O. Box 587, FIN-40101 Jyväskylä, Finland

ABSTRACT

Reference geometries consisting of a constriction block and a secondary pipe were used to provide reference information for estimation of the performance of more complex geometries resembling to real headbox designs. This information included the fluidisation ability curves, i.e. the minimum attained floc size in function of mechanical energy loss, the rate of fluidisation in sudden expansion, the rate of subsequent reflocculation and the level of saturation floc size. The functionality of this approach was illustrated with measured information of a particular complex geometry on several research environments of different scale. By paper samples produced with a similar geometry, the tight connection of the fluidised state of the suspension and of the attained formation was verified. Reduction of the residence time of suspension in the headbox resulted to lower floc size in slice lip area and to better level of formation in produced paper. In addition, both properties revealed a similar form for this dependency. By changes on tensile strength ratio of the produced paper, the operation of the forming section was shown to have an apparent but not controlling effect on the level of formation obtained.

1 INTRODUCTION

Of the numerous descriptive parameters of paper properties the non-uniform basis weight distribution, i.e. formation, constitutes a useful view. Many functional properties are dependent on formation, e.g. tensile strength, cockling and print uneveness. The formation attained in a paper machine depends on both the fluidised state of the suspension delivered by the headbox and on the operation of the former [1]. The main physical phenomena related to a conventional former are the shear field generated by the jet-to-wire speed difference and the hydrodynamic smoothing on the forming section. While it is not possible to prevent these characteristic phenomena to effect the formation, for the purpose of the experiments, the former can be run in a sense of minimum interference. This leaves the state of suspension in the slice jet as the dominating property. On the other hand, fibres in a wood pulp suspension have a strong tendency to stick together to form inhomogeneous flocculated networks [2,3], i.e. flocs, which are known to be an important factor in leading to bad formation. Therefore, the knowledge of fluidisation and reflocculation behaviour of the suspension in the headbox should provide predictive means to estimate attainable formation with different designs and operational parameters. In this study, it is shown that changes in formation follow the predicted state of fluidisation also in practice.

At fibre consistencies that exceed the sedimentation consistency, fluidisation and the associated breakage of flocs is attained by inducing turbulent flow. In a headbox, turbulence is created by wall shear and by sudden expansion steps. By these means, the initial fibre structure is first broken into smaller flocs and single fibres with weakly correlated velocities. Due to the presence of fibres, turbulence is effectively damped leading to fast re-growth of floc size in the decaying turbulent field. Floc size distribution and velocity fluctuations are thus indicative of the degree of fluidisation [4]. Accordingly, these properties are used to describe the fluidised state of suspension through the entire study. The evolution of floc size was measured using a fast shutter CCD-camera with transmitted light and appropriate image analysis [5] and the turbulent state of the fibrous phase was characterised by capturing velocity fluctuations of fibres with pulsed ultrasound-Doppler anemometry (PUDA) [6,7]. With this procedure, the fluidised state of suspension, i.e. the fluidisation and reflocculation behaviour, was determined both for simple constriction blocks of circular cross section, i.e. reference geometries (RGs), and geometries resembling real headbox channels. With a set of specifically dimensioned RGs it was possible to construct reference curves (RCs) corresponding to a range of geometric dimensions in order to judge the fluidisation behaviour in the more complex geometries (CGs). The RC information included, e.g. the minimum floc size attained with a specific constriction block geometry in function of the head loss (Figure 10), the rate of fluidisation in sudden expansion (Figure 9), the rate of subsequent reflocculation (Figure 14) and the level of saturation floc size (Figure 17). With this information, the floc size evolution in a headbox can be predicted in a wide range of operational parameters. Paper samples, equivalent to regular LWC base paper, were then produced in a pilot machine environment with headbox geometry corresponding to the CG. The attained formation in these runs was determined by the standard β-formation analysis of paper samples. Consequently, these results were used to evaluate the prediction obtained from the fluidisation behaviour.

It is shown that by these specifically designed experiments on fluidisation and reflocculation the time evolution of the suspension can be determined. There, the reference geometries are used to provide the RCs and to reveal the limitations set by the geometric dimensions of the channel, e.g. the saturation floc size and the corresponding reflocculation time. By repeating the same kind of analysis in real headbox geometries of higher complexity and by taking into account the reference information, the type of fluidisation behaviour can be determined (Figure 21). The obtained information then includes both the time evolution of fluidised state and the possible existence of limiting phenomena. With representative paper samples, the tight connection of the fluidised state of the suspension and the formation was verified. In addition, changing of some operational parameters of the headbox were shown to lead differences in formation in line with the predicted change of the fluidised state of suspension (Figure 24). This ability to predict formation characteristics is extremely useful for the product development and design of both the headbox and the former. Operation and control of the paper machine would benefit by obtaining proper guidelines for adjustments.

2 EXPERIMENTAL APPROACH

2.1 Analysis of suspension flow

Three different pulps were used as the fibre phase. Two of them consisted of bleached chemical hardwood pulp (M1, M2) and one of them was based on bleached chemical softwood pulp (M3). All three pulps were unbeaten and contained no fillers or added chemicals. Characteristic properties of these pulps are given in Table 1 together with the value of crowding factor [8]

$$N_{cf} = \frac{2}{3} C_v \left(\frac{l_f}{d_f} \right)^2 \approx \frac{5 C_m l_f^2}{\omega}. \tag{1}$$

In Equation (1) C_V denotes volumetric consistency, C_m mass consistency, l_f length-weighted average fibre length, d_f average fibre diameter and ω coarseness. According to the classification made by Kerekes and Schell [8], pulp suspensions with the crowding factor in the range from 1 to 60 belong to the regime of “forced collisions”, which is the operational range covering most wet-end processes. The values of crowding factor for the three pulps used in these experiments are close to each other. Consequently, a qualitatively same kind of behaviour in fluidisation and reflocculation were expected.

The results concerning the flow and state of suspension were based on three types of measurements: floc dimensions by an image analysis arrangement, turbulent intensity of fibre phase by pulsed ultrasound-Doppler anemometry and loss of mechanical energy by differential pressure transmitters. A short description of each method is given in the following chapters.

Table 1 Characteristic properties of pulps used in experiments.

Pulp	Average fibre length l_f [mm]	Average fibre diam. d_f [μm]	Coarseness ω [mg/m]	Consistency C_m [%]	Crowding factor N_{cf}
Hardwood kraft (Birch) M1	0.96	18.9	0.114	1.0	40.4
Hardwood kraft (Birch) M2	0.89	19.4	0.106	1.0	37.4
Softwood kraft (Pine) M3	2.09	29.2	0.221	0.5	49.4

2.1.1 Floc size

A schematic illustration of the imaging arrangement is shown in Figure 1. In the arrangement, a fast shutter CCD-camera was used to acquire images and the suspension was illuminated from the opposite side of the test geometry by a DC regulated plane light source [5]. To avoid smear in high speed conditions, e.g. at the slice lip area, the arrangement was supplemented with LCD shutter, installed between the CCD sensor and optics. The shutter allowed

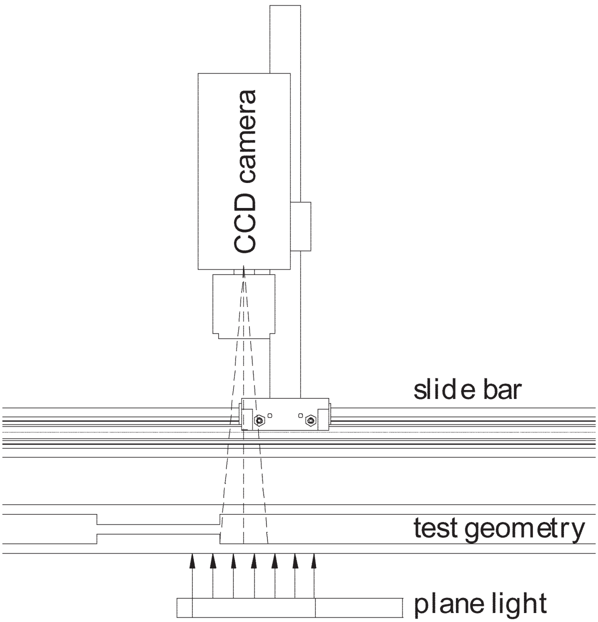

Figure 1 Imaging arrangement for floc size measurements.

construction of pulsed illumination in which the rising edge of a pulse was created with a reset signal to the sensor and the falling edge with closing of the shutter. A computer-controlled slide bar carried out positioning of the frame in which the camera and the light source were attached.

Although high quality light sources were utilised in experiments, variations of illumination field existed in test sections because of the illumination distribution of the light source itself, of the varying optical properties in test sections and of a variable depth of suspension between the camera and the light source. Therefore, the acquired images were enhanced by a procedure based on an assumption of constant mass flux across the image area and on the Lambert Beer's law (*2*) for the intensity of transmitted light

$$I(z) = I_0 e^{-\alpha C_m z}. \tag{2}$$

In Equation (2), I_0 is the intensity of incident light, z is the depth of the suspension, α is the decay constant and C_m is the mass consistency of the suspension. Thus, in the enhancement procedure the distribution in the recorded mean illumination field is eliminated from the original images according to the equation

$$I_{ij}^{E,k} = \langle I_s \rangle \frac{I_{ij}^{k}}{\exp(\langle \ln I \rangle_{ij})}, \tag{3}$$

where $I_{ij}^{E,k}$ represent the enhanced image sequence. In this notation, i and j refer to pixel indices and $k = 1 \ldots N$ denotes the number of images in the sequence. Further, I_{ij}^{k} refers to the original sequence, $\langle I_s \rangle$ stands for the average grey level of the sequence and $\langle \ln I \rangle$ is the average of logarithms of the sequence. An example of an original and an enhanced image is shown in Figure 2.

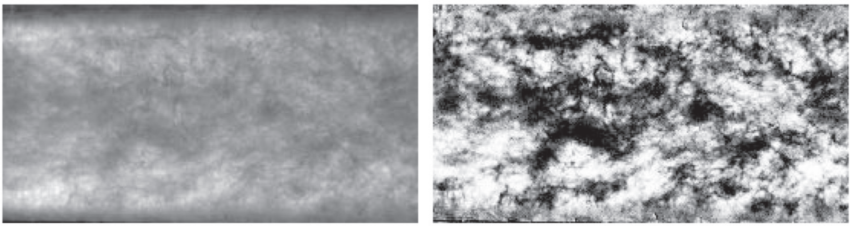

Figure 2 Original image and image after enhancement procedure for floc size analysis.

To determine the floc size from the enhanced images, a threshold operation with the median of intensity was carried out in a way that 50% of the image area was marked as flocs and 50% as voids. The distribution of floc dimensions in both stream-wise (MD) and span-wise (CD) directions were then computed for every image in the sequence as the run-length distributions $\hat{f}(L_x)$ and $\hat{f}(L_y)$. To achieve an appropriate number of samples these distributions were finally averaged to produce the smooth distributions $f(L_x)$ and $f(L_y)$ shown in Figure 3.

By assuming cylindrical symmetry of flocs a dimensionless floc volume V_f^* was defined with the equation

$$V_f^* = \frac{\langle L_x \rangle \langle L_y \rangle^2}{l_f^3}, \tag{4}$$

where $\langle L_x \rangle$ and $\langle L_y \rangle$ are length-weighted average floc dimensions in MD and

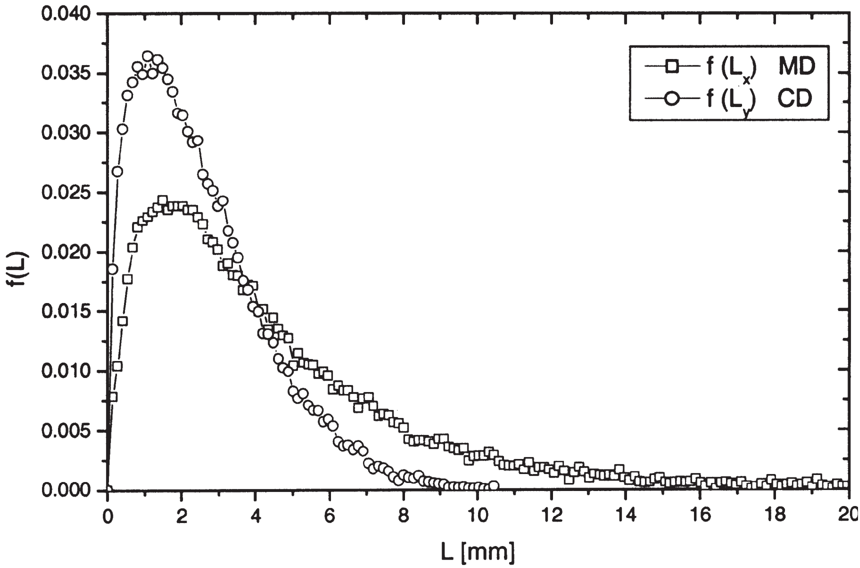

Figure 3 Distributions of stream-wise and span-wise floc size distributions from 200 images.

CD, respectively, and l_f is the length-weighted average fibre length of suspension.

2.1.2 Turbulence of fibre phase

The turbulent state of fibre phase was characterised by measuring velocity fluctuations of fibres with DOP 1000, a pulsed ultrasound-Doppler anemometer (PUDA) from Signal Processing S.A. This device exploits a single transducer, the 4 MHz Standard series TR1 transducer in these experiments, for emitting and receiving ultrasound pulses (Figure 4). The instantaneous beam-wise velocity component at a location on the path of the ultrasound beam is obtained from the Doppler frequency shift of the echoed pulses induced by the moving fibres. Intensity of turbulence, defined as

$$I(u_f) = \frac{\sqrt{\frac{1}{N-1} \sum_{N}^{i=1} (u_{f,i} - U_f)^2}}{U_f}, \tag{5}$$

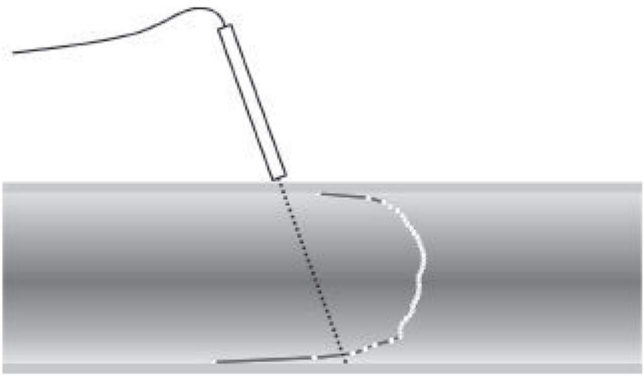

Figure 4 Transducer of PUDA and measured average velocity profile.

was utilised as the particular parameter describing the turbulent state of fibre phase. In Equation (5), u_f and U_f are used to stand for the instantaneous and mean values of fibre phase velocity. Data from 500 consecutive profiles, each of them consisting of 32 fast repetitions, served as the base for intensity calculations.

2.1.3 Loss of mechanical energy

The loss of mechanical energy in sudden expansion of the constriction block was determined with Valmet-Rosemount Model 3051C differential pressure transmitter (Figure 5). The calibrated accuracy of the transmitters was better than $\pm 0.1\%$ of full range. Pressure differences were recorded as a function of flow rate with small steps through the entire flow range used in experiments. The frictional loss in primary and secondary pipes between the capillary tubes, $\Delta h_{f,pipe1}$ $\Delta h_{f,pipe2}$, were removed from the recorded values, as well as the dynamic pressure at the location of pressure tappings

$$\Delta h_f = \frac{dp}{\rho g} + \frac{V_1^2 - V_2^2}{2g} - \Delta h_{f,pipe1} - \Delta h_{f,pipe2}. \tag{6}$$

In Equation (6), Δh_f represents the loss of mechanical energy in sudden expansion.

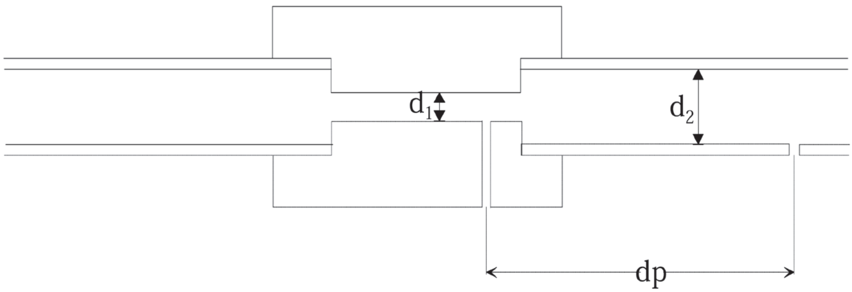

	PPP1	PPP2	PPP3	PPP4
d1 [mm]	11.4	15	18.6	15
d2 [mm]	16	21	26	26

Figure 5 Dimensions of constriction blocks with secondary pipe (RGs) and location of capillary tubes for head loss measurement.

2.2 Paper samples

The paper produced on the pilot paper machine was regular LWC base paper having a basis weight of 40 g/m^2 and an ash content of 10%. The length-weighted mean fibre length and the CSF level of the used furnish, brought from a nearby production machine, were 1.85 mm and 152 ml, respectively.

Two different approaches were used to produce a range of mean residence times for the suspension in the headbox. In the first set (set 1), the flow rate entering the headbox was considered as the only variable resulting to a simple variation of residence time with a fixed geometry. The main problems related to this approach were in the difficulty to maintain a constant jet-to-wire speed ratio and to keep the operation of the forming section similar with a large range of flow rates. To enhance the similarity in forming, the second set (set 2) was run by adjusting simultaneously the slice opening and the machine speed while going through the range of flow rates. This facilitated the operation of the forming section but, at the same time, induced slight variations in the slice chamber geometry. The other running parameters of the pilot paper machine were kept as constant as possible during all tests. Especially, the twin wire roll-blade former used in the tests was run in a sense of minimal interference, i.e. the operational parameters of the components on the forming section were kept unchanged and they were chosen so that the effect of drainage elements on the forming paper web was minimised. In addition, the retention and tensile strength ratio of paper were observed during the tests and a certain value, acceptable for the LWC base paper in question, was tried to maintain. Regardless of this monitoring, slight variation of retention and tensile strength ratio between recorded test points remained due to the complexity of their on-line control. Some deliberate deviations from the ideal state also emerged, e.g. to guarantee runnability, the vacuum level of the forming roll was elevated on large flow rates.

The tensile strength and the β-formation were measured from the produced paper samples. These properties were analysed by the automated paper testing equipment PaperLab and the Ambertec Formation Analyzer, respectively. Both devices use standard methods for determination. In addition, an analysis of the grain size distribution for a selected set of paper samples was also performed. In this analysis, the digitised β-radiogram of a paper sample was used to provide information analogous to the sequence of enhanced images in the floc size analysis of suspension. This image information was then converted to a quantitative form with an image analysis procedure almost equivalent to that used for suspension [5]. The actual motivation for this analysis was to provide information of paper samples corresponding better to the floc size analysis of suspension.

2.3 Research environments

The experiments were carried out in three environments of different scale. A small scale flow loop capable of producing flow rates up to 3.5 l/s were utilised for experiments in the scale of a single turbulence generator tube. A laboratory scale flow loop extending to flow rates 40 l/s were applied for small bundles of turbulence generator tubes and for a corresponding section of slice chamber. Experiments for a narrow but otherwise complete headbox were accomplished in a pilot scale flow loop. This environment was capable of producing flow rates up to 250 l/s/m. The largest environment, used to produce paper samples, consisted of a pilot paper machine. The experiments in this environment included flow rates as high as 290 l/s/m.

3 RESULTS

3.1 Reference geometries (RGs)

3.1.1 Fluidisation in sudden expansion

A lot of research has been conducted on the flow over a sudden expansion, i.e. a backward-facing step (BFS). These studies have mostly been concentrating on two-dimensional steps but, although differences exist, the results are also applicable to axisymmetric steps (ABFS) in many aspects [9,10]. The flow field behind the step is quite complex and detailed information has become available mainly by the development of two and three-dimensional optical flow field measurement systems [11,12] and direct numerical simulation (DNS) [13,14]. Despite of the embedded complexity, some features of the flow in ABFS can be expressed in a simple form. The loss of mechanical energy can be calculated with the Borda-Carnot equation

$$\Delta h_f = \zeta \frac{V_1^2}{2g}. \tag{7}$$

In Equation (7) V_1 denotes the mean velocity in the entering flow, i.e. in the primary pipe, and ζ represents the loss coefficient. For a wide range of velocities V_1 and ratio of cross-sectional areas A_1/A_2, the loss coefficient can be accurately predicted with

$$\zeta = \left(1 - \frac{A_1}{A_2}\right)^2 = \left(1 - \left(\frac{d_1}{d_2}\right)^2\right)^2. \tag{8}$$

This expression has been shown to be valid also for pulp suspension flows. The considerable loss of mechanical energy in ABFS is related to the back-flow eddy behind the step. By reducing the momentum of this eddy the energy consumption of ABFS can be lowered. Several mechanisms have been introduced in the literature [15,16].

As a results of the back-flow eddy an intense shear field is created on the mixing layer between the eddy and the entering flow. It is known from experiments for pure fluids that the highest values of this stress field are found slightly up-stream of the reattachment point of the eddy. An increased mechanical energy loss by higher velocity (7) or larger ratio of cross-sectional area (8) is realised as a more intensive stress field. This dependency is illustrated in Figure 6a and 6b.

Fluidisation of the entering suspension is achieved by the stress field created since the minimum of axial floc size evolution is detected at the same

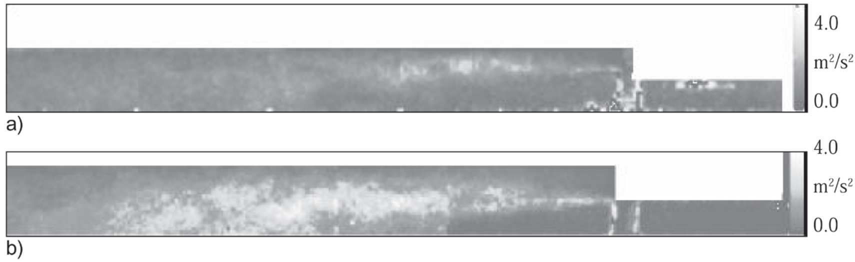

Figure 6 Kinetic energy of turbulence $k = \frac{1}{2}(u_l^2 + v_l^2)$ in two ABFS of different dimensions (mm): a) $d_1/d_2 = 15/22.6$ and b) $d_1/d_2 = 16/25.6$; u_l and v_l are velocity fluctuations in plane of DPIV measurements and flow is from right to left $Q = 1.5$ l/s.

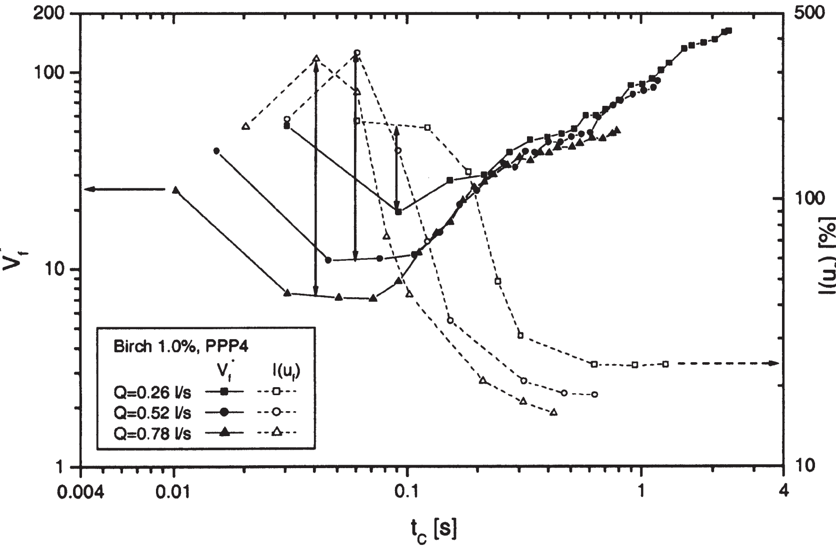

Figure 7 Approximate co-location of minimum floc size and peak of turbulent intensity; reference geometry PPP4 with bleached hardwood pulp 1.0%.

approximate location as the highest turbulent intensity of the fibre phase (Figure 7). A visual study confirms that this axial location also corresponds approximately to the mean reattachment point of the back-flow eddy. In Figure 7, and here onwards, x_C and $t_C = x_C/V_2$ correspond to the axial distance and to the mean residence time from the expansion of ABSF.

On these basis, changes in the consumption of mechanical energy of the ABSF are expected to lead discernible differences in the fluidisation of the suspension. More specifically, a higher loss of mechanical energy should yield to a smaller floc size.

The evolution of measured floc size in axial direction (MD) for the RG PPP3 have been presented in Figure 8. As discussed above, the minimum of each curve represents the approximate mean length (reattachment point) of the back-flow eddy. It is seen that, as for pure fluids, this mean length does not much depend on the flow rate. Up-stream of this point the floc size decreases and correspondingly fluidisation occurs. Down-stream of the reattachment point reflocculation is seen to initiate. The general trend of floc size evolution existing in Figure 8 can be perceived also from the results on flocculation

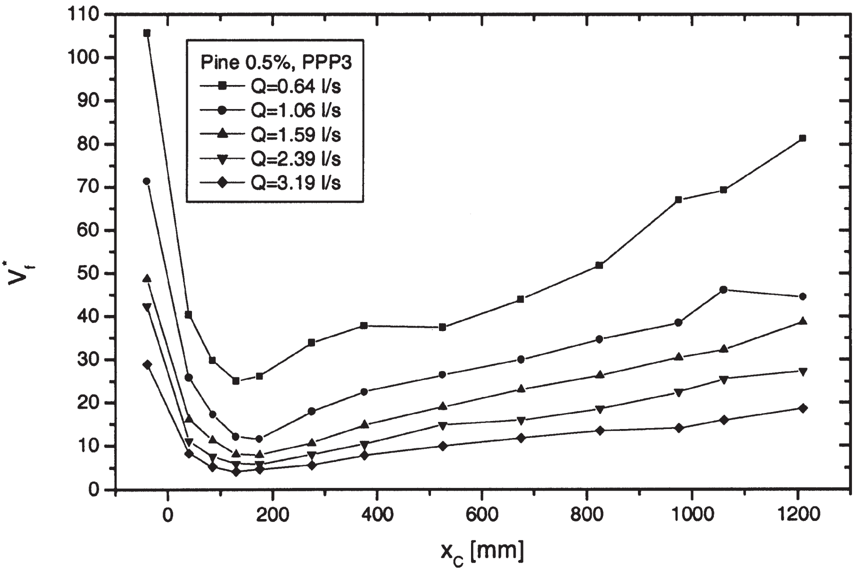

Figure 8 Evolution of floc size in function of axial distance from step expansion; reference geometry PPP3 with bleached softwood pulp 0.5%.

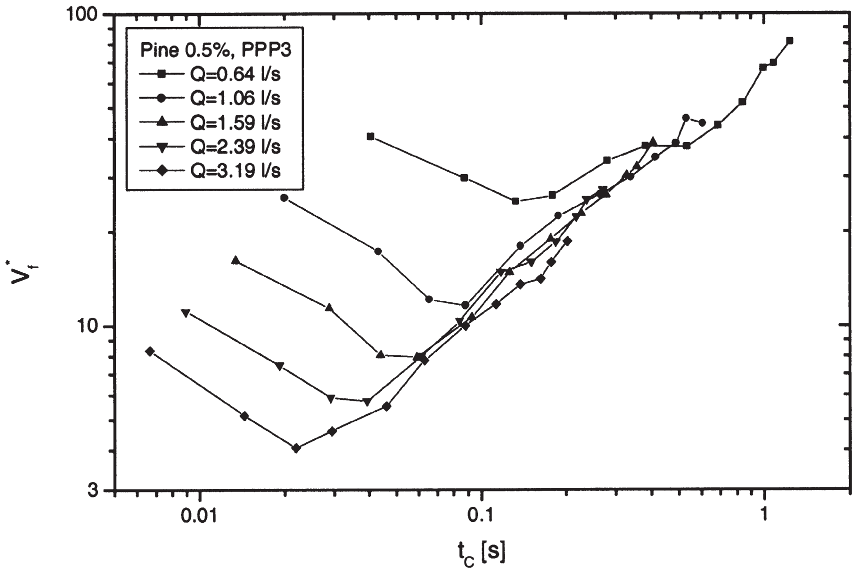

Figure 9 Evolution of floc size in function of mean residence time from step expansion; reference geometry PPP3 with bleached softwood pulp 0.5%.

obtained with another experimental approach utilising the concept of flocculation intensity [17].

It has been shown in an earlier publication [1] that it is useful to present the axial evolution of floc size as a function of mean residence time instead of the axial distance (Figure 9). This reveals the importance of t_C as the independent variable in fluidisation and reflocculation. In a double logarithmic scale, the fluidisation curves are seen to be roughly collinear lines for all flow rates.

A useful view of the fluidisation ability of an ABFS, shown in Figure 10, can be obtained by picking up the minimum floc size (at point of reattachment) of each curve and plotting them as the function of corresponding expansion loss, defined by Equation (7). Clearly, a higher loss of mechanical energy in an ABFS results to the smaller floc size, i.e. to the better fluidisation. In addition, the fluidisation efficiency of a particular ABFS reduces considerably as the flow rate increases.

By presenting the fluidisation ability curves, like in Figure 10, of all RGs in a same picture with double logarithmic scale leads to a set of approximately collinear lines. This means that the fluidisation ability curves can be represented by an equation of the form

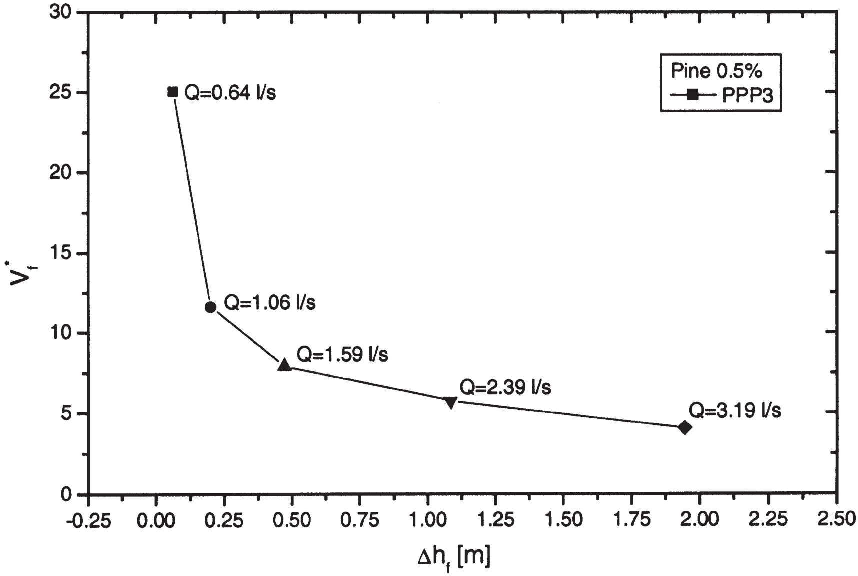

Figure 10 Minimum floc size in function of expansion loss; reference geometry PPP3 with bleached softwood pulp 0.5%.

$$\frac{V_f^*}{V_{f,0}^*} = c\left(\frac{\Delta h_f}{\Delta h_{f,0}}\right)^{-b}, \tag{9}$$

where the subscript notion 0 refers to the value at the level of the lowest energy loss, common to all RGs. The exponent b of the function (9) can be found on this double logarithmic scale by the linear interpolation

$$\log_{10}\left(\frac{V_f^*}{V_{f,0}^*}\right) = -\, b\log_{10}\left(\frac{\Delta h_f}{\Delta h_{f,0}}\right) + \log_{10}(c), \tag{10}$$

as illustrated in Figure 11. To complete the non-linear function (9), the non-dimensional floc size is set to approach asymptotically the value one as energy loss is increased

$$\Delta h_f \rightarrow \infty\,, V_f^* \rightarrow 1. \tag{11}$$

In this way, the final form of the fluidisation ability curve for an ABFS can be written as

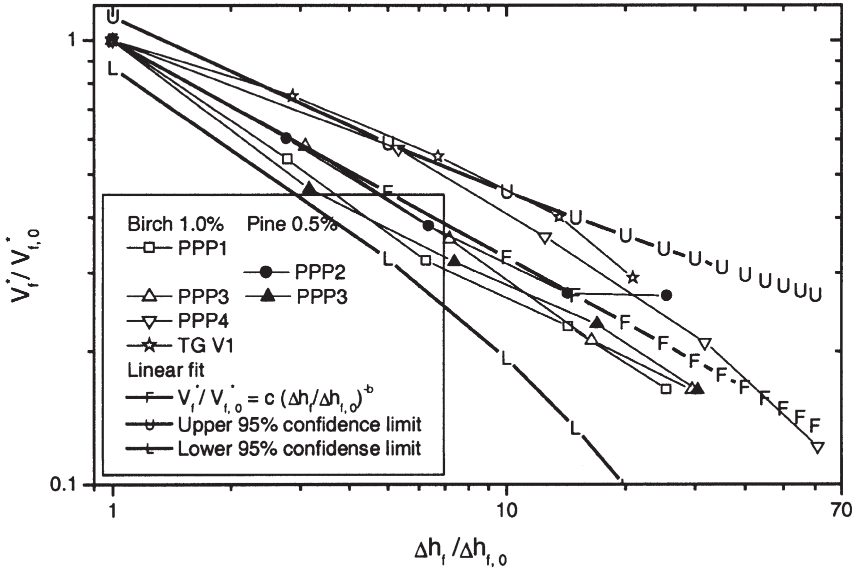

Figure 11 Minimum floc size in function of expansion loss; scaling of Δh_f and V_f* by values with lowest energy loss, RGs PPP1 to 4 and CG TG V1 with bleached softwood pulp 0.5% and bleached hardwood pulp 1.0%.

$$V_f^* = cV_{f,0}^* \Delta h_{f,0}^b \Delta h_f^{-b} + 1 = a\Delta h_f^{-b} + 1. \tag{12}$$

The fluidisation ability curves with the non-linear fit of the form (12) have been shown in Figure 12. Clearly, the approach described above provides a method to predict the fluidisation ability of an ABFS and, accordingly, sets a well-defined point for the subsequent reflocculation analysis.

It is assumed that the length scale of turbulence and the dimensions of flocs have to be at the same order of magnitude for fluidisation to occur. Considerably larger flow structures would only transfer the flocs from point to point and notably smaller structures would not be able to cause stresses at the size of flocs. Accordingly, the most active length scale in breaking flocs will vary as the fluidisation proceeds. The large scales acting as the source of turbulent energy are characterised by the step size of an ABFS but the small scales are set by the amount of turbulent energy fed at large scales. This means that the increase in flow rate will result in broadening of the spectrum towards the small scales. In turbulent flow all length scales from the large to

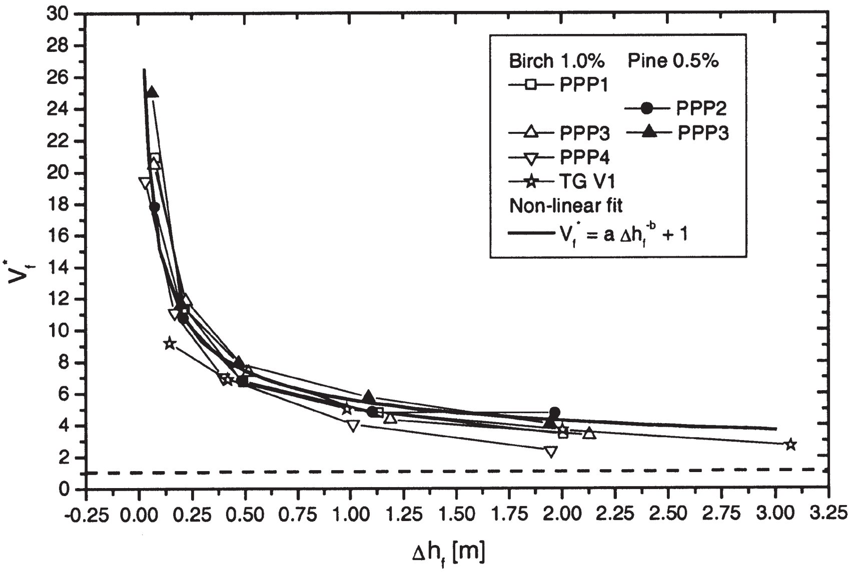

Figure 12 Measured minimum floc size and non-linear fit in function of expansion loss; RGs PPP1 to 4 and CG TG V1 with bleached softwood pulp 0.5% and bleached hardwood pulp 1.0%.

the dissipative scales exist but the steepest gradients are found at the Taylor's micro-scale. Thus, the reduction of fluidisation efficiency of an ABFS with increasing flow rate may originate either from the change in the active length scale of turbulence or from the higher strength of smaller flocs. As discussed above, the large scale end can be varied by the step size and the small scale end by the flow rate.

A set of three RGs, i.e. PPP1, PPP2 and PPP3, each of them having the same ratio of cross-sectional areas $A_1/A_2 = 0.51$, were used to obtain more information on this subject. According to Equation (8) the RGs should have the same loss coefficient. This was verified by measuring the expansion loss Δh_f with a large range of flow rates for all three RGs. Then, the axial floc size evolution was determined with the same five values of Δh_f in each RG by adjustment of the flow rate. With this approach it was possible to vary both the large scale and the small scale ends of turbulent spectrum. Therefore, changes in the fluidisation ability between the RGs should be observed if the compliance of the active length scale of turbulence and the dimensions of flocs would be the main issue. Figure 12 reveals that practically the same fluidisation ability is reached with this set of three RGs. This result is considered to indicate that the strength of flocs increases as their size decreases.

Two suspensions, bleached hardwood pulp of 1.0% and bleached softwood pulp of 0.5%, were used for which the crowding factor N_{cf} is approximately equal. It is seen from the Figure 12 that the same fluidisation ability, expressed with the dimensionless floc volume V_f^*, is obtained for both suspensions. This emphasises the importance of fibre length as the controlling parameter in fluidisation.

3.1.2 Reflocculation

After the point of highest stresses and the minimum floc size the suspension begins to reflocculate as indicated in Figure 13. As no geometric restrictions exist at first, this process is termed as the area of *free growth*. It is seen that from the point of minimum floc size all the curves collapse into a common line that gives the time evolution of floc size. This indicates that, in the area of free growth, the floc size depends only on the mean residence time t_C.

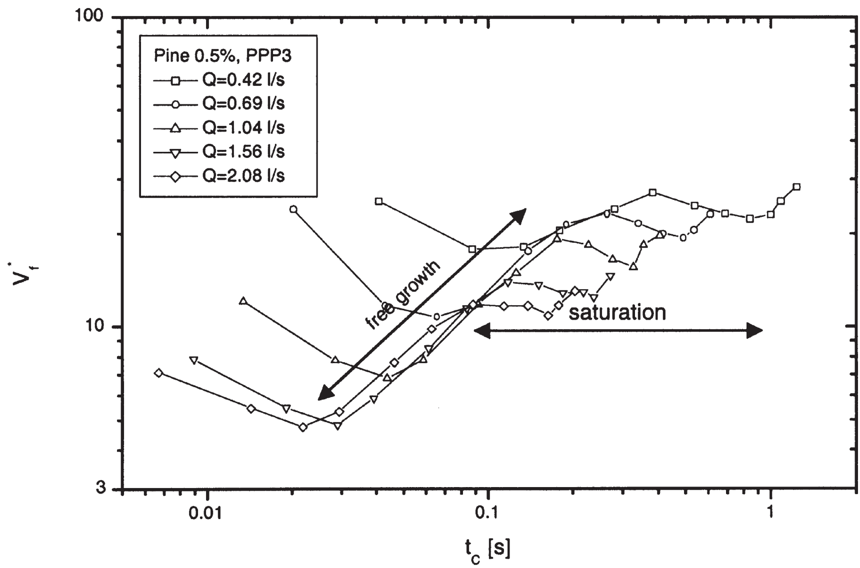

Figure 13 Areas of free growth and saturation; RG PPP2 with bleached softwood pulp 0.5%.

Thus, the process of reflocculation can be described with the following simple equation

$$V_f^* = a(t_C - t_{C,0})^b, \tag{13}$$

where $t_{C,0}$ takes into account the position of the minimum floc size downstream of the expansion. Physically, the behaviour of suspension seen in Figure 13 means that the process of reflocculation is independent of the initial state of flocs. Therefore, the fibre phase do not seem to have a memory of the past and the only difference between the floc size evolution curves is in their different entry point to the common reflocculation curve, corresponding to the amount of mechanical energy loss in the expansion.

The importance of the turbulent scales on fluidisation was studied above with the RGs PPP1, PPP2 and PPP3 having the same ratio of the cross-sectional areas. Similarly, this set of RGs provided here means to have an understanding on their importance to reflocculation. In Figure 14, the area of free growth of the floc size evolution curves has been shown separately. The data from RGs PPP2 and PPP3 have been complemented with the fit of

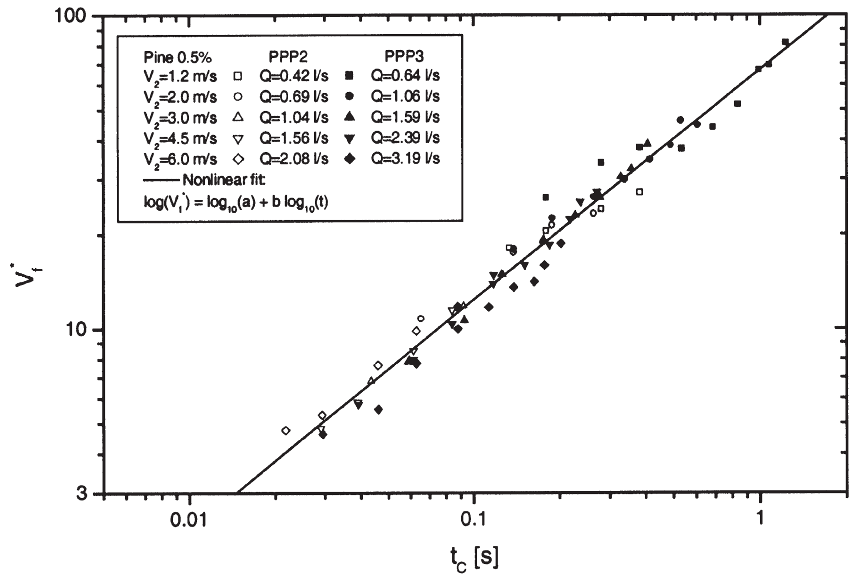

Figure 14 Rate of reflocculation with different scales of turbulence; RGs PPP2 and PPP3 with bleached softwood pulp 0.5%.

the Equation (13). On the used double logarithmic scale, the slope b of the line

$$\log_{10}(V_f^*) = b\log_{10}(t_C) + \log_{10}(a) \tag{14}$$

directly represent the rate of reflocculation. It is realised, as for the fluidisation, that the variation of the turbulent scales at both the large and small scale ends have no primary importance.

A collection of data from RG PPP3 with bleached hardwood and softwood pulps have been shown in Figure 15. Although the crowding factor N_{cf} for these two pulps is approximately the same, the ratio of the expansion step size to their mean fibre length is 1.77 and 3.85, respectively. Nevertheless, no apparent differences between reflocculation of the pulps exist. This indicates that at least for pulps with a similar crowding factor the reflocculation behaviour may be universal. It also shows that the fibre length is the dominating scale in the initial reflocculation process. Consequently, the relative rate of floc growth is independent of the fibre length.

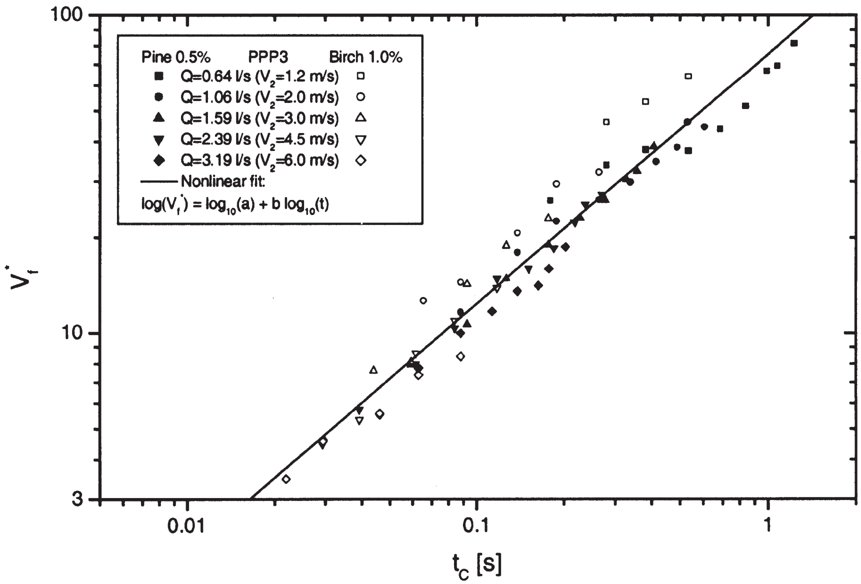

Figure 15 Rate of reflocculation with different ratio of turbulent length scale and fibre length; RG PPP3 with bleached softwood pulp 0.5% and bleached hardwood pulp 1.0%.

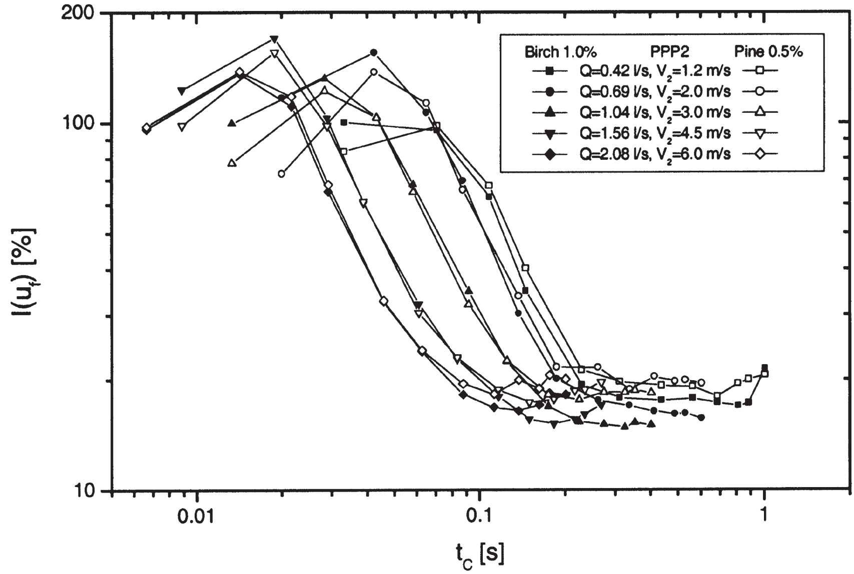

Figure 16 Decaying of fibre phase intensity for suspensions of same N_{cf}; RG PPP2 with bleached softwood pulp 0.5% and bleached hardwood pulp 1.0%.

Next, the above results on reflocculation are supplemented by measurements of the turbulent intensity of the fibre phase. This reveals that the velocity fluctuations in the fibre phase are rapidly decreasing while the floc size is increasing (Figure 16). In the double logarithmic scale the curves of intensity, in the area of free growth, are almost collinear lines. The same results are obtained with both pulps of the almost equal N_{cf}.

By plotting the curves of intensity together with the floc size evolution (Figure 17) reveals that both properties begin to level off approximately at the same residence time, dependent on the flow rate. This means that for longer residence times the flow realises the geometric limitations set by the channel size and, correspondingly, the state of suspension begins to approach the developed state of channel flow. Consequently, this value of residence time is used to separate the areas of free growth and saturation.

3.1.3 Saturation

In the area of saturation, the decaying of turbulence have proceeded so far that the production in the wall layer of the channel begins to limit further

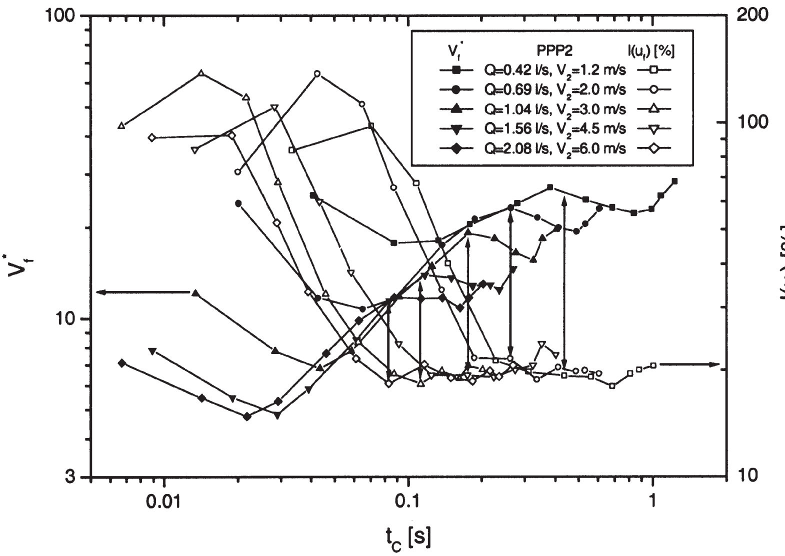

Figure 17 Level off of floc size and intensity marking start of saturation; RG PPP2 with bleached softwood pulp 0.5%.

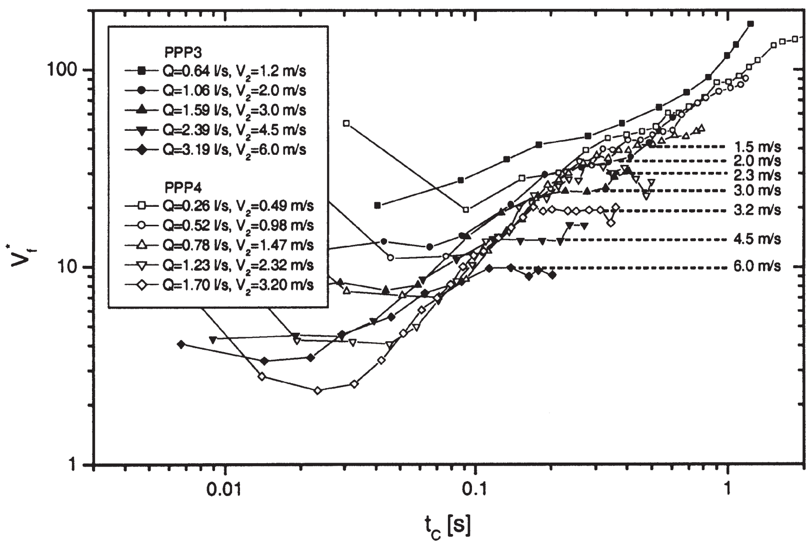

Figure 18 Dependency of saturation floc size on velocity; RGs PPP3 and PPP4 with bleached hardwood pulp 1.0%.

reduction of intensity. Because of this production, further growth of floc size is prevented and an approach to the saturation floc size, characteristic to the channel flow and fibre suspension, is realised.

For a particular channel size d_2 the frictional resistance and, correspondingly, the production of turbulence increases with velocity. Thus, reduced saturation floc size is expected as the flow rate is increased. In Figure 18, data for RGs PPP3 and PPP4 having equal size of secondary pipe d_2 are shown. Although the expansion step size of the RGs is different, the saturation floc size is seen to grow systematically with decreasing velocity.

As the RGs PPP1, PPP2 and PPP3 were set for the same ratio of cross-sectional areas and as they were measured with equal loss of mechanical energy, the same mean velocity in the secondary pipe V_2 was achieved. Accordingly, they provide a natural basis to gain an understanding on the effect of pipe diameter d_2 for the saturation floc size. Figure 19 reveals that a strong dependency is found in which the saturation floc size increases with the diameter.

In fluidisation and in reflocculation the same behaviour was achieved with suspensions of an equal crowding factor. However, this similarity does not

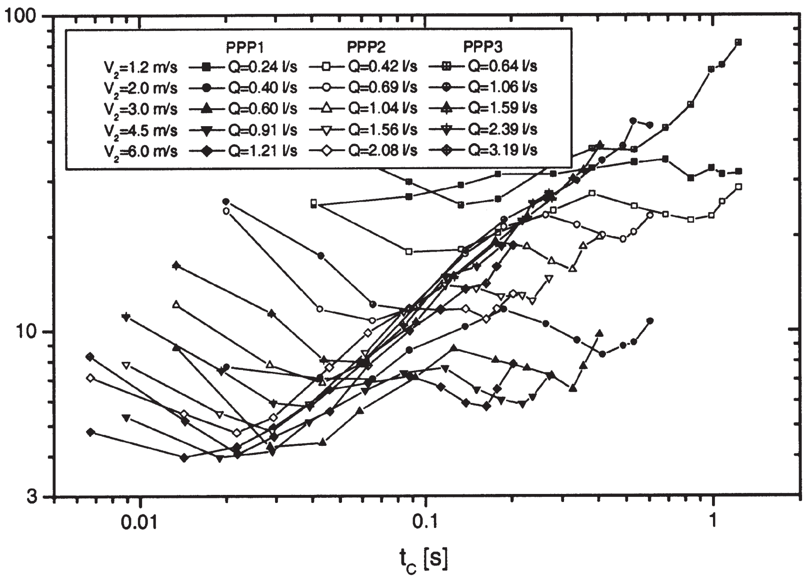

Figure 19 Dependency of saturation floc size on pipe diameter; RGs PPP1, PPP2 and PPP3 with bleached softwood pulp 0.5%.

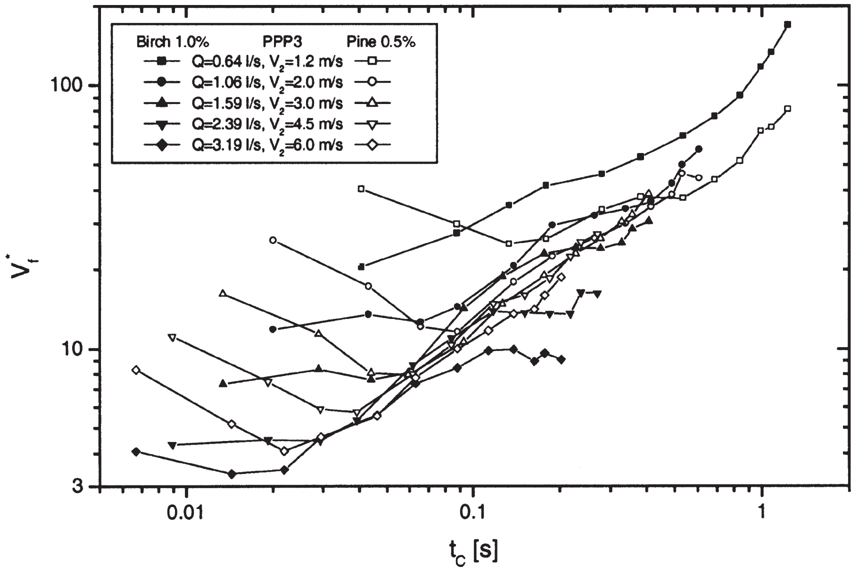

Figure 20 Saturation floc size with different ratio of turbulent length scale and fibre length; RG PPP3 with bleached softwood pulp 0.5% and bleached hardwood pulp 1.0%.

hold for the saturation size as seen from Figure 20. The softwood pulp of higher fibre length does not yet experience saturation as for the hardwood pulp the state of saturation is already reached at high velocities.

3.2 Complex geometry (CG)

The procedure described here necessitates the measurement of RCs for the suspension of desired fibre type and consistency. This is not a serious restriction though as the required information is quite limited in extent.

The fluidisation behaviour of a more complex geometry can now be estimated quite easily with the RC information from the geometrically simple RGs. In general terms this task consists of three stages. At first, the fluidisation ability of a CG with different flow rates is calculated from the loss of mechanical energy (12). In this way, the entry point to the reflocculation curve is determined. At second, the residence time of flow in a CG is calculated for all desired flow rates. The state of fluidisation corresponding these flow rates is then found from the equation of reflocculation (13). At third, the

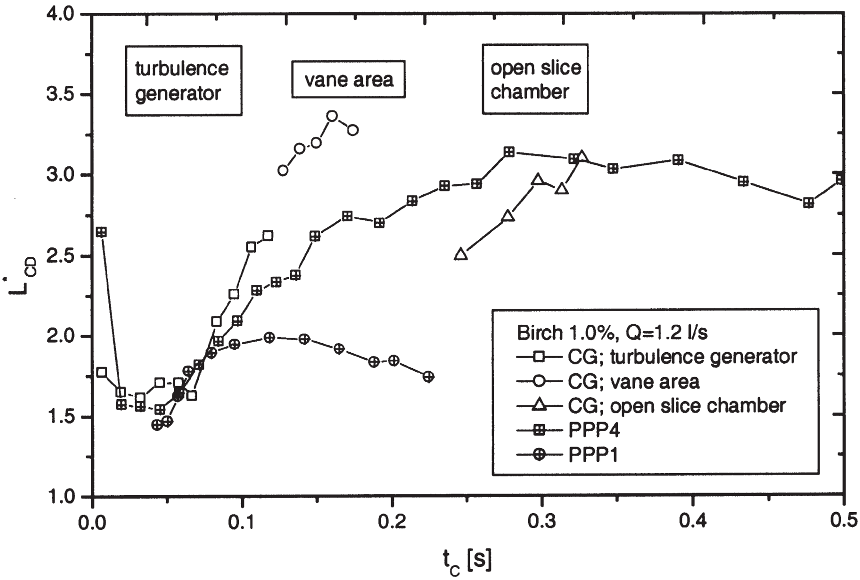

Figure 21 Performance of CG compared to RGs at flow rate 1.2 l/s/ pipe; bleached hardwood pulp 1.0%.

information on the saturation floc size is examined for encountering the limitations to floc growth.

The above procedure should not be expected to provide an accurate and reliable estimation on the performance of a CG without measured information of floc size evolution in the actual geometry but it provides a useful tool in making reasoned decisions of the headbox design beforehand. An example of the floc size behaviour of a particular CG in reference to the RCs for two flow rates (residence times) is given in Figure 21 and Figure 22. Different parts of the floc size evolution curve for the CG represent measurements at the small scale, the laboratory scale and the pilot scale environments, respectively.

The RG PPP4 is used here as the appropriate reference as this geometry provides equivalent performance of fluidising section, i.e. constriction part of the turbulence generator. Since the CG includes long vanes in the slice chamber a model for the small scale environment, consisting of a singly turbulence generator tube and a part of the slice chamber, can be made to represent the full scale model almost up to the lip area. In addition, a laboratory scale

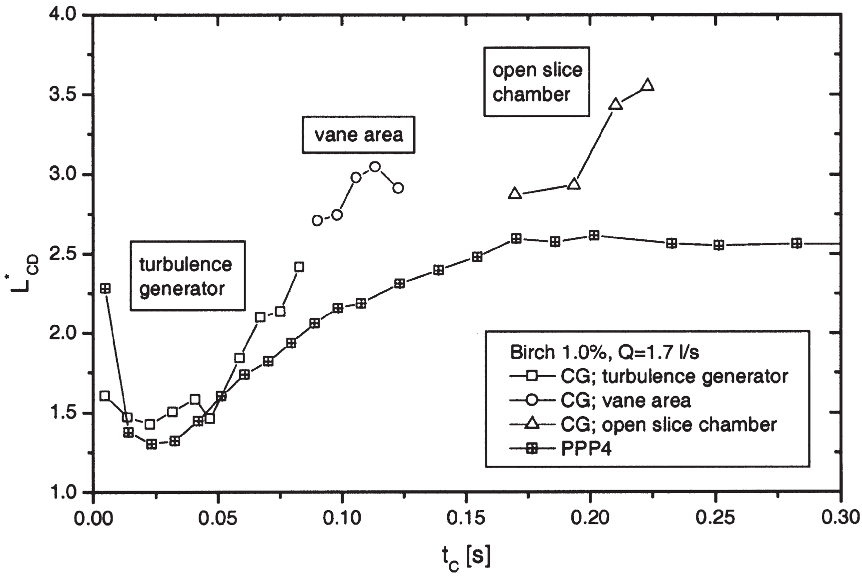

Figure 22 Performance of CG compared to RGs at flow rate 1.7 l/s/pipe; bleached hardwood pulp 1.0%.

model has been used to collect the data in the slice chamber area and a pilot scale model was utilised for recording the floc size at the lip area.

At both flow rates, 1.2 and 1.7 l/s per turbulence generator tube, the CG performs similarly. In the turbulence generator part, the development of floc size follows quite closely the appropriate RG. The slightly faster reflocculation rate is a consequence of the acceleration in this part. The same phenomenon can be seen at the end of the slice chamber after the vanes. Further, in both areas the rate of reflocculation is approximately the same. As a whole, the behaviour of the CG resembles quite well the general trend predicted by the RG. The analysis is completed by including the floc size evolution curve of the RG PPP1 in the same picture with the other data. This RC is used to provide the saturation floc size information appropriate for the channel dimensions at the vane area. Clearly, the floc size evolution of the CG does not meet limitations from saturation.

3.3 Prediction of paper formation

As the floc size of the suspension delivered by the headbox is considered as the main parameter controlling the formation of the produced paper, reduced floc size at the lip area of the slice chamber should result in better formation of the paper. With a particular geometry, smaller floc size is obtained by reducing the residence time of suspension in the headbox. This is demonstrated by Figure 23 in which the measured floc size of CG at the lip area in function of the residence time is shown.

The Ambertec formation measured from the paper samples produced with a headbox closely resembling the CG used in the flow analysis has been shown in Figure 24. A reference to Figure 23 reveals that a similar trend in floc size and in formation is obtained in function of the residence time. The resemblance with the set 1 is seen to be more accurate. This is in line with expectations since the set 1 was ran with lower tensile strength ratio than the set 2. As the tensile strength ratio is related to the jet-to-wire speed difference the lower formation levels in set 2 reflect the activity of the forming section.

An additional verification of the tight connection of the fluidisation level

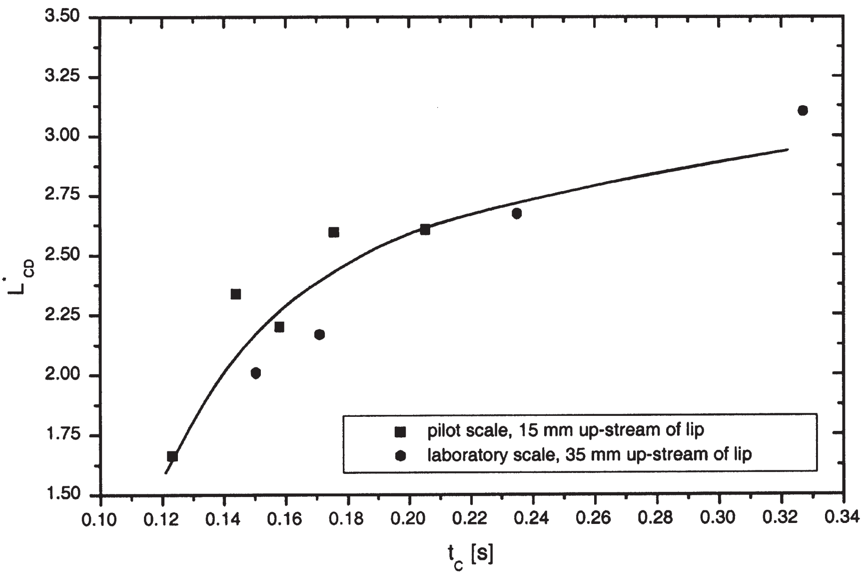

Figure 23 Floc size of CG at lip area for different residence times of suspension in headbox; 15 mm (pilot scale) and 35 mm (laboratory scale) up-stream of lip.

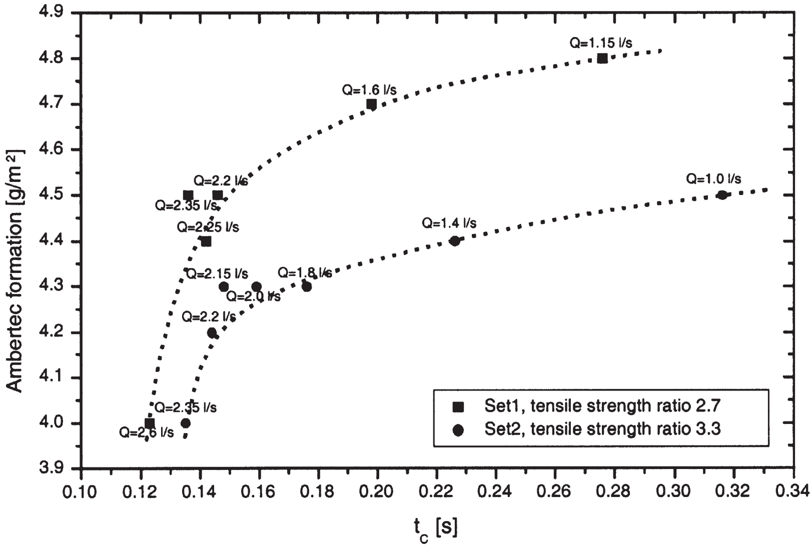

Figure 24 Ambertec formation for different residence times of suspension in headbox; CG with LWC furnish.

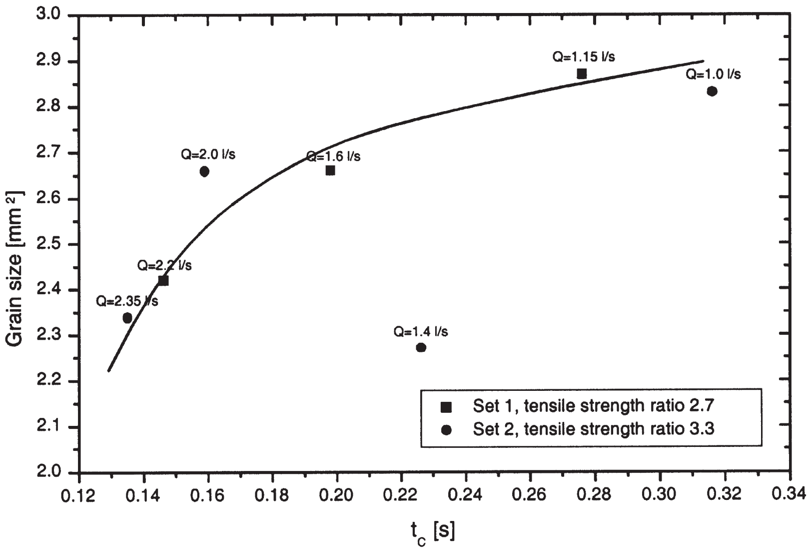

Figure 25 Grain size of digitised β-radiograms for different residence times of suspension in headbox; CG with LWC furnish.

and the homogeneity of the mass distribution in paper was obtained by the results of the grain size analysis of the β-radiograms. The results in Figure 25 represent a selected subset of the samples in Figure 24. It is noticed that the results of set 1 and set 2 combine again to a common trend line as for the floc size at the lip area (Figure 23). To further illustrate the close resemblance with the results of these two analyses, the trend line of Figure 23 has been shown also in Figure 25.

4 CONCLUSIONS

The geometrically simple reference geometries (RGs), consisting of a constriction block and a secondary pipe, were used to provide reference curves (RCs) for estimation of the performance of more complex geometries (CGs) resembling to real headbox designs. The RC information included the fluidisation ability curves, i.e. the minimum floc size in function of mechanical energy loss, the rate of fluidisation in sudden expansion (ABFS), the rate of reflocculation and the level of saturation floc size.

Several results concerning the behaviour of pulp suspensions in RGs were obtained. The combined measurements of floc size and local turbulent intensity of fibres revealed that the fast decrease of floc size in the fluidisation region after a sudden expansion was accompanied by a simultaneous increase of fibre phase turbulent intensity. The minimum floc size and the maximum intensity were located at the same stream-wise position downstream of the ABFS. This location was considered to represent the approximate length of the back-flow eddy. When the minimum floc size was expressed in function of the loss of mechanical energy in ABFS a simple power law dependency was found. This dependency was shown to be practically independent on the scales of turbulence and on the ratio of turbulent scales and fibre length. In addition, two different pulps with equal crowding number obeyed the same dependency. Further downstream of the location of minimum floc size a region of reflocculation was found where the floc size gradually increased and the turbulent intensity decreased. This was termed as the area of free growth. In this regime, the floc size scaled by the mean fibre length followed a common dependency on time for all three pulps studied here. In particular, the reflocculation process seemed to be independent of the initial state of fibre phase and of the turbulent scales set by the ABFS. In the area of free growth, the floc size depended on time according to a power law. It was shown that a particular length of the area of free growth existed which was determined by decaying of the fibre phase turbulent intensity at the level limited by the production of turbulence at the wall layer. This condition was then used to separate the area of free growth from the area of saturation. A dependency both on velocity and channel size existed in which a decrease of saturation floc size with an increase of velocity and an increase of saturation floc size with larger channel size prevailed, respectively.

With these specifically designed experiments on fluidisation and reflocculation in RGs, the time evolution of fluidised state and the possible existence of limiting phenomena were determined. Then, the fluidisation behaviour of a more complex geometry was estimated with the created RC information. The functionality of this approach was illustrated with measured information of a particular CG on several environments of different scale. By paper samples produced with a similar CG, the tight connection of the fluidised state of the suspension and of the formation was verified. Reduction of the residence time of the suspension in the headbox resulted to lower floc size and to better formation level together with a similar form of this dependency. In addition, by changes on tensile strength ratio the operation of the forming section was shown to have an apparent but not controlling effect on the level of formation obtained.

5 REFERENCES

1. Niskanen K., Kajanto I. and Pakarinen P., "Paper structure in Paper physics", Edited by K. Niskanen, Published by Fapet Oy in series of Papermaking Science and Technology, 15–51 (1998).
2. Kerekes, R. J., "Pulp Flocculation in Decaying Turbulence", *J. Pulp Pap. Sci. 7*, TR86–TR91 (1983).
3. Norman, B., "Turbulence and flocculation measurements in fibre suspensions. International Symposium on Papermachine Headboxes" (Invited lecture). McGill University, Montreal, 1979.
4. Karema, H., Kataja, M., Kellomäki, M., Salmela, J. and Selenius, P., "Transient fluidisation of fibre suspension in straight channel flow", TAPPI International Paper Physics Conference, September 26–30 1999, San Diego, USA, 369–379 (1999).
5. Kellomäki, M., Karema, H., Kataja, M., Salmela, J. and Selenius, P., "Fibre flocculation measurement in pipe flow by digital image analysis", TAPPI International Paper Physics Conference, September 26–30 1999, San Diego, USA, 461–463 (1999).
6. Ricker, N.L. and Forster, F.K., "Pulse Doppler ultrasonic velocity measurement in aqueous pulp fiber suspensions", *Tappi J.*, **68**(1): 79–82 (1985).
7. Takeda, Y. "Velocity profile measurement by ultrasonic Doppler method", Experimental Thermal and Fluid Science 10: 444–453, 1995.
8. Kerekes, R. J. and Schell, C. J., "Characterization of fibre flocculation regimes by a crowding factor", *J. Pulp Pap. Sci.*, **18**(1): J32–38 (1992).

9. Papadopoulos, G. and Ötügen, M.V., "Separating and reattaching flow structure in a suddenly expanding rectangular duct", *Journal of Fluids Engineering*, 117, 17–23 (1995).
10. Hertzberg, J.R. and Ho, C.M., "Three-dimensional vortex dynamics in a rectangular sudden expansion", *J. Fluid Mech.*, 289, 1–27 (1995).
11. Shih, C. and Ho, C.M., "Three-dimensional recirculation flow in a backward facing step", *Journal of Fluids Engineering*, 116: 228–232 (1994).
12. Kasagi, N. and Matsunaga, A., "Three-dimensional particle-tracking velocimetry measurement of turbulence statistics and energy budget in a backward-facing step flow", *Int. J. Heat and Fluid Flow*, **16**: 477–485 (1995).
13. Kaiktsis, L., Karniadakis, G.E. and Orszag, S.A., "Unsteadiness and convective instabilities in two-dimensional flow over a backward-facing step", *J. Fluid Mech.*, 321, 157–187 (1996).
14. Le, H., Moin, P. and Kim, J., "Direct numerical simulation of turbulent flow over a backward-facing step", *J. Fluid Mech.*, 330, 349–374 (1997).
15. Kim, B.N. and Chung, M.K., "Experimental study of roughness effects on the separated flow over a backward-facing step", *AIAA Journal*, **33**(1), 159–161 (1994).
16. Heenan, A.F. and Morrison, J.F., "Passive control of backstep flow", *Experimental Thermal and Fluid Science*, **16**: 122–132 (1998).
17. Raghem-Moayed, A. and Kuhn, D.C.S., "Turbulent flocculation measurement", *J. of Pulp and Paper Science*, **26**(4): 163–165 (2000).

Transcription of Discussion

PREDICTION OF PAPER FORMATION BY FLUIDISATION AND REFLOCCULATION EXPERIMENTS

Hannu Karema[1], *Juha Salmela*[1], *Maarit Tukiainen*[2] *and Hannu Lepomäki*[2]

[1]VTT Energy

[2]Metso Paper Oy

Dick Kerekes University of British Columbia

You mention in your paper mechanical friction loss Δh_f which equals a coefficient multiplied by $V^2/2g$ and then you talk about the turbulence you measured. Did you measure any pressure losses to determine their loss of energy? The Δh_f is for the total loss after the contraction over a long distance. Did you measure any local losses? Did you measure any pressure losses at all?

Hannu Karema

Yes. Referring to Figure 5 in the paper the pressure loss is measured across the changes of diameter.

Dick Kerekes

Do you have the dimensions in your paper I didn't get a chance to see where the pressure taps were?

Hannu Karema

I really don't remember, where these dimensions are given in the paper – I will have to check; but they were measured over the contraction and then over this part (referring to Figure 5) and the third position was the expansion for which we have to include the back flow eddy. This is the scale of the pressure measurements. They are not global ones.

Discussion

Dick Kerekes

So it is just for the constriction as a whole.

Bill Sampson Department of Paper Science, UMIST

Have you looked at fibre geometry and fibre stiffness, also fibre flexibility, which I suspect may start to influence the flocculation rate?

Hannu Karema

Certainly other things than mean fibre length influence on fluidisation and reflocculation. But their effect seems to have minor importance. We didn't want to include such things in this presentation.